Opt Quant Electron (2018)50:117
https://doi.org/10.1007/s11082-018-1387-2

Dynamic mesh grids for laser head tomography

Huseyin Ozgur Kazanci[1]

Received: 26 December 2016 / Accepted: 12 February 2018
© Springer Science+Business Media, LLC, part of Springer Nature 2018

Abstract In this work, new image reconstruction schema has been proposed for back-reflected diffuse optical tomography geometry. 100 source and 100 detector points have been selected as bifurcated probe positions in xy plane. An x, y, and z cubic coordinate grid system has 10 × 10 × 30 mesh grids. In this work, a dynamic mesh grid concept has been introduced first. Each time source and detector positions are changed, x and y coordinate positions have been reassigned automatically. Centers between source and detector positions have been recalculated in xy plane. x and y grid positions have been reassigned around this center points. When using *predefined* static mesh grid photon fluencies which are coming from Monte Carlo (MC) simulation output or diffusion equation are transferred into static voxels which is only partially correct. Hence there is no symmetry around source–detector matchup center in xy plane and so is not totally correct. In this work, dynamic mesh grids have been created and photon fluencies have been assigned into automatically redefined dynamic mesh grid voxels. One dimensional depth profile has been used for simplicity. Median values of transport functions for each z depth grids have been used. Transport functions of photon fluencies from each source to detector positions have been calculated and each voxel value has been assigned in three dimensional dynamic mesh grid array. We innovated the use of dynamic mesh grid array instead of using static mesh grids which were being used previously, and now have assigned the photon fluencies into the dynamic mesh grid voxels. This also gave us an opportunity to use different transport functions for one dimensional image reconstruction schema. Before, we were using the sum of transport weight functions which are derived from each of the z depth layers. Now we have opportunity to use mean or median values also. Thus we are centering the dynamic mesh grid array by finding the center of each source and detector position successfully. This work gave us encouragement to build tomography devices.

✉ Huseyin Ozgur Kazanci
ozgurkazanci@akdeniz.edu.tr; ozgurkazanci@gmail.com

[1] Department of Biomedical Engineering, Faculty of Engineering, Akdeniz University, 07058 Antalya, Turkey

Published online: 15 February 2018

Keywords Dynamic mesh grid array · Back-reflected laser head tomography model · Monte Carlo modeling of light transport (MCMLT) · Tikhonov inverse problem solution algorithm · Image reconstruction

1 Introduction

The main task of this work has been testing the new forward model approach to diffuse optical tomography (DOT) biomedical imaging devices and showing the result based on the multi layered head simulation model. Basically DOT imaging modality has two mathematical basics, one is forward model generation and the other is inverse problem solution. Then, the inverse problem solution is being used for image reconstruction. Molecules under the tissue surface are visualized by reconstructing the images. Forward model is created by the linearized physical or natural behavior of migrating photons inside the imaging tissue. Photons are penetrating inside the tissue according to the diffusion approximation of a nuclear radiative transport equation. This has a nonlinear form which decays by the time and distance exponentially. Nonlinear form of the photon penetration is not easy to solve by the mathematical solution methods. Typically, instead of using the nonlinear migration form, the linearized equation system is used. Linearized equation system is the first Taylor term of Rytov and Born Approximation of Radiative Transport Equation which is the derivative form of the nuclear radiative transport equation. This equation system can be defined as in Eq. 1 (Kazanci and Jacques 2015; Kazanci 2015a, b; Kazanci and Canpolat 2014, 2015a, b; Kazanci et al. 2015).

$$y = Ax. \tag{1}$$

In this equation system, $\boldsymbol{A}$ is the total transport functions from source to detector positions which is defined as a forward problem in literature. The $\boldsymbol{x}$ is the optical properties of dynamic mesh grid array voxels. The values of $\boldsymbol{x}$ are the unknowns. They should be solved by inverse problem solution algorithms. $\boldsymbol{Y}$ is the data which is acquired by tomography devices or artificial data which can be created by simulation programs such as which we have created in this work. When creating artificial y data, matrix multiplication is usually done. The unknown optical properties are optical absorption coefficients over background which are defined by $\Delta\mu_a$.

2 Materials and methods

2.1 Forward model

Pre-defined head layers have been built for the simulation setup using a seven layer model. ANSI C Monte Carlo modeling of light transport (MCMLT) simulation code has been run and photon fluence ratios have been generated by this program code. In Table 1, tissue types, thickness and optic coefficients have been given. The seven defined layers are hair, epidermis, dermis, skull, cerebrospinal fluid (CSF), gray matter, and white matter tissues by the order of from outer to inner. Absorption coefficient of hair is $\mu_a = 26\ cm^{-1}$, scattering coefficient of hair is $\mu_s = 107\ cm^{-1}$, anisotropy coefficient of hair is $g = 0.9$, slab thickness of hair is 100 μm. Absorption coefficient of epidermis is $\mu_a = 4.6\ cm^{-1}$, scattering coefficient of epidermis is $\mu_s = 250\ cm^{-1}$, anisotropy coefficient of epidermis is $g = 0.9$, epidermis slab thickness epidermis is 100 μm. Absorption coefficient of dermis is

Table 1 Tissue types

Tissue	Hair (100 μm)	Epidermis (100 μm)	Dermis (1 mm)	Skull (5 mm)	CSF (5 mm)	Gray matter (5 mm)	White matter (…–3 cm)
μ_a (cm^{-1})	26	4.6	0.05	0.016	0.026	0.07	0.07
μ_s (cm^{-1})	107	250	140	195	0.015	107	107

$\mu_a = 0.05\ cm^{-1}$, scattering coefficient of dermis is $\mu_s = 140\ cm^{-1}$, anisotropy coefficient of dermis is $g = 0.9$, slab thickness of dermis is 1 mm. Absorption coefficient of skull is $\mu_a = 0.016\ cm^{-1}$, scattering coefficient of skull is $\mu_s = 195\ cm^{-1}$, anisotropy coefficient of skull is $g = 0.9$, slab thickness of skull is 5 mm. Absorption coefficient of CSF is $\mu_a = 0.026\ cm^{-1}$, scattering coefficient of CSF is $\mu_s = 0.015\ cm^{-1}$, anisotropy coefficient of CSF is $g = 0.95$, slab thickness of CSF is 5 mm. Absorption coefficient of gray matter is $\mu_a = 0.07\ cm^{-1}$, scattering coefficient of gray matter is $\mu_s = 107\ cm^{-1}$, anisotropy coefficient $g = 0.9$, Gray matter slab thickness is 5 mm. Absorption coefficient of white matter is $\mu_a = 0.07\ cm^{-1}$, scattering coefficient of white matter is $\mu_s = 107\ cm^{-1}$, anisotropy coefficient of gray matter is $g = 0.9$, slab thickness of white matter is upto 3 cm.

Photon fluencies have been generated by given cylindrical radial r and depth z mesh grid coordinate distances by using ANSI C MCMLT photon simulation program with time mode selection. Generated photon fluencies have been transferred to MatLAB™ programming environment. Source and detector positions have been selected as seen in Fig. 1. Between each source and detector position transport functions have been calculated based on the dynamic mesh grid array voxel positions. Each time the source and detector positions have been changed, the dynamic mesh grid array voxel positions have also been

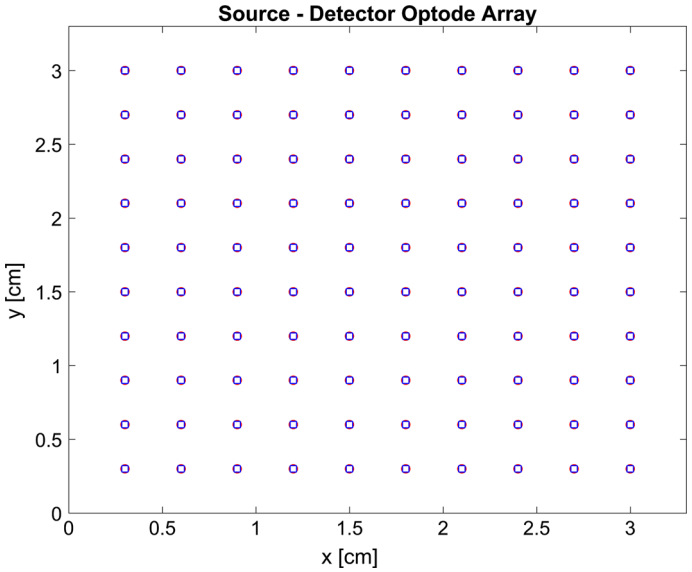


Fig. 1 Sources and detectors

redefined and photon fluence ratios have been interpolated with the (r, z) cylindrical mesh grid data. 100 source and 100 detector positions have been used as seen in Fig. 1. x, y grids are 3 cm. 10 × 10 × 30 x, y, and z grids have been selected. Depth is 2 cm. Top view of transport function between 1st source and 100th detector is presented in Fig. 2. The photon fluencies symmetry can be seen from figure.

Side view of the transport functions between 1st source and 100th detector can be seen in Fig. 3. This figure has also symmetry between source and detector.

In Figs. 4, 5, and 6 first 10, 100 and all source–detector pairs the sum, mean, and median of weights along the depth z profile can be seen. These three kind of weights have been tested while making transport functions in the forward model and inverse problem solution algorithm. In this work, one-dimensional image reconstruction algorithm has been applied instead of using three-dimensional approach. In one-dimensional approach three different weight schema have been applied to the forward model and inverse problem solution algorithm as well. Sum is the sum of forward model transport functions in each step of one-dimension which is along the z depth profile in this example. For each z depth profile, all transport functions have been summed. In Figs. 4, 5, and 6 the sum of weights along the z depth profile can be seen. In the middle of figures, mean values of source–detector matches along the z depth profile can be seen. And finally median value which is the center of source–detector matches of weight functions along the depth z profile can be seen at the bottom of figures.

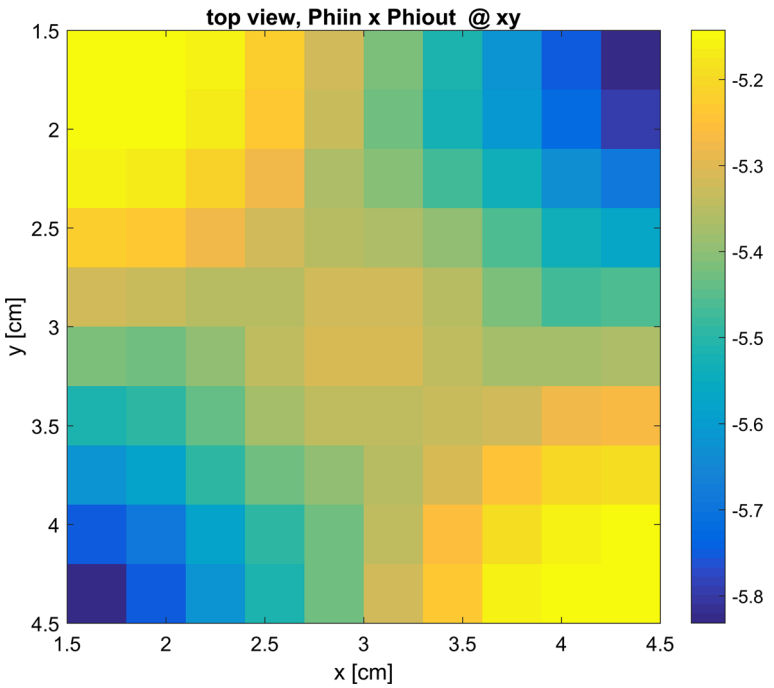


Fig. 2 Top view of transport functions between 1st source and 100th detector

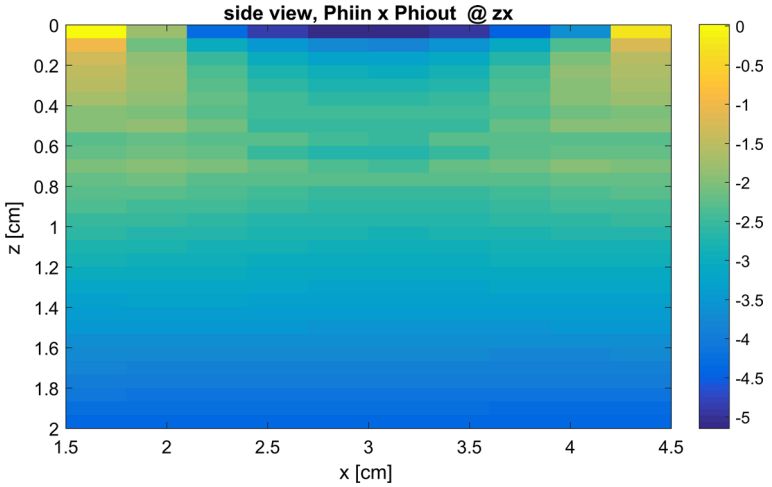


Fig. 3 Side view of the transport functions between 1st source and 100th detector

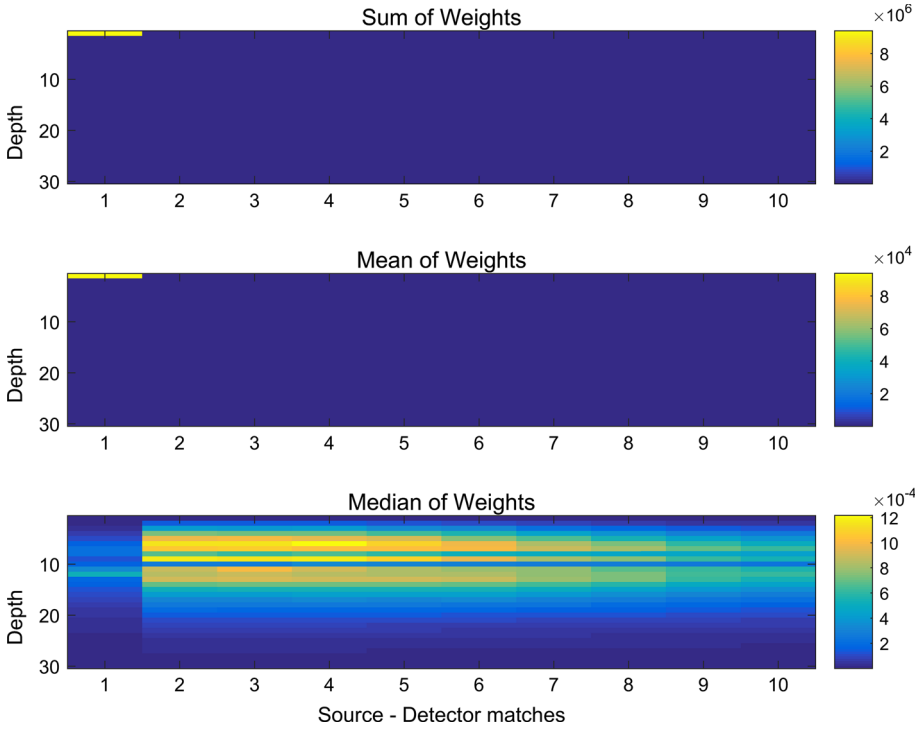


Fig. 4 First 10 source–detector matches sum, mean, and median of weights along the depth z profile

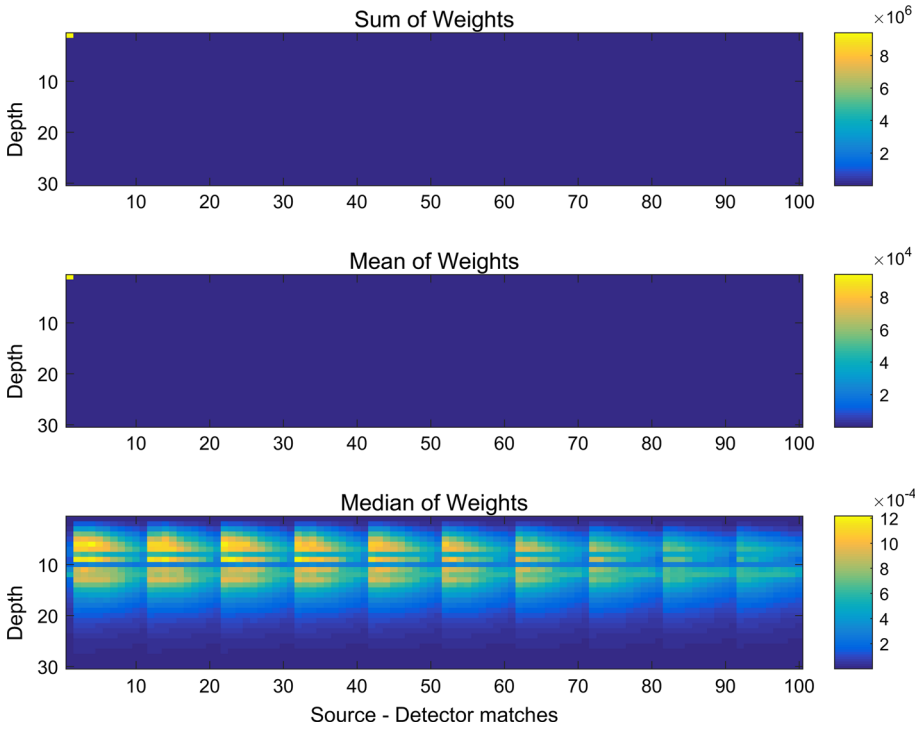


Fig. 5 First 100 source–detector matches sum, mean, and median of weights along the depth z profile

3 Results

Inclusion was buried into 29 different depth levels up to 20 mm which can be seen from Fig. 7. For each depth layer, real inclusion position has been shown by dashed red line and reconstructed images have been presented by bar graph. Images have been reconstructed by using median transport functions of source–detector matches along the z depth profile. Tikhonov inverse problem solution algorithm has been selected for inverse problem solution as shown in Eq. 2 (Kazanci and Oduncuoglu 2015, 2016; Kazanci 2015c, 2016a, b, c, d). λ parameter has been selected as $\lambda = 10^{-12}$. Unknown delta absorption concentration has been calculated as $\mu_a = 0.001\ \text{cm}^{-1}$.

$$x = \left(A^T A + \lambda I\right)^{-1} A^T y \tag{2}$$

Reconstructed image and concentration is the same as real location and concentration up to 20 mm depth.

4 Discussion

In this work, dynamic mesh grids have been used for the first time. The previous works had been done with the static mesh grid arrays. Static mesh grids are using grids which are not changed even when the source and detector positions are changed in xy grids. If the source

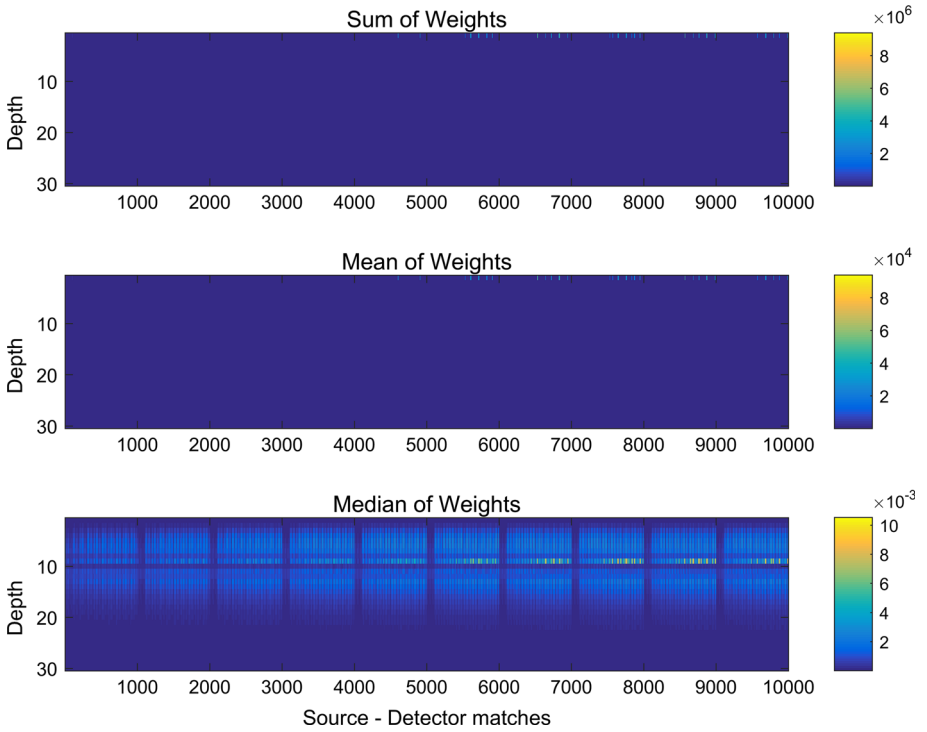


Fig. 6 All source–detector matches sum, mean, and median of weights along the depth z profile

and detector positions stay in the corner of static mesh grid array then we cannot use transport functions inside the forward model which are beyond the edge of geometry which should actually be employed. On the other hand, dynamic mesh grid array method uses beyond the edge of static mesh grid array hence, it is changing mesh grids automatically when the source and detector positions change. It is finding the center of each source–detector match in xy grids then by using this center it is distributing the positions of mesh grids based on this center. This method is more accurate than any other static mesh grid methods. As long as we use dynamic mesh grid array method, we can easily select median of transport functions between each of the source and detector matches. In one-dimensional approach, one-dimensional depth profile has been thought from the view of unknown space. Each z profile has been thought as one unknown. 20 mm has 29 unknowns which is representing z depth profile. A one-dimensional approach is also quick method for testing purpose. The real question and discussion can be evaluated here, whether using median of transport functions along the z depth profile with dynamic mesh grid array correct or not? The answer may be given indirectly. Is using sum of weights along z depth profile approach correct naturally for the one dimensional problem? The answer is no. Because between each of the source–detector pair in mesh grid, the photons which are collected in the detector side cross mostly between their middle point transactions rather than the very far away point. This also answers the real question. What is the middle point transactions between each source and detector match? The answer is the median of transport functions along the z depth profile between source and detector match. In this work, image reconstruction is made using median of transport functions between source and detector pairs in

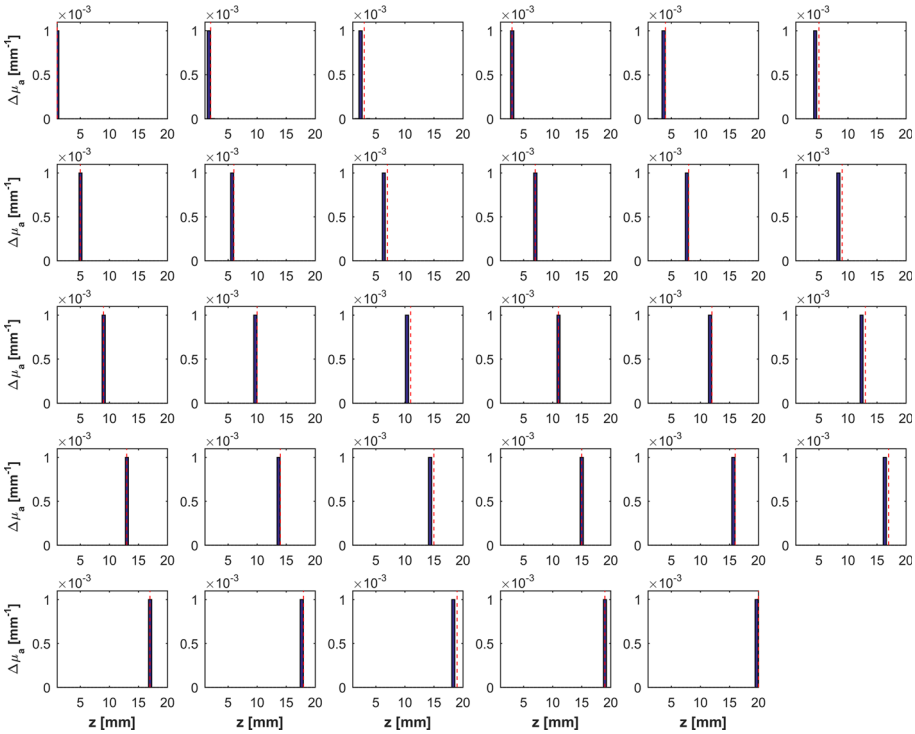


Fig. 7 Reconstructed image along depth z profile with real positions (dashed red lines). (Color figure online)

forward model generation and using it in inverse problem solution algorithm by Tikhonov inverse problem solution algorithm as presented.

5 Conclusion

In this work, the new dynamic mesh grid array approach for forward model transport functions generation has been done. Median values have been used first. Dynamic mesh grid array has been used first. Dynamic mesh grids are useful when selecting the median of transport functions along the depth z profile, hence the geometrical middle point of transport functions vector is the best selection for a one-dimensional image reconstruction method. Dynamic mesh grid method is more accurate than previously used static mesh grid array method. In the upcoming studies, it is presumed that dynamic mesh grid method will be used.

Compliance with ethical standards

Conflict of interest The author declares that he has no competing interests.

References

Kazanci, H.O.: Weight matrix analysis for back reflection continuous wave diffuse optical tomography (CWDOT) systems: translational method. Opt. Quantum Electron. **47**(12), 3847–3853 (2015a)

Kazanci, H.O.: Designing intact clinical head laser tomography system. In: Proceedings of IEEE Medical Technologies National Conference (TIPTEKNO). 2015 October 15–18; Bodrum, Mugla, Turkey. IEEE, pp. 280–283, 36720, (2015b). https://doi.org/10.1109/tiptekno.2015.7374104

Kazanci, H.O.: Development of coordinate definition algorithm for head laser tomography system. In: Proceedings of IEEE Medical Technologies National Conference (TIPTEKNO). 2015 October 15–18; Bodrum, Mugla, Turkey. IEEE, pp. 276–279, 36720, (2015c). https://doi.org/10.1109/tiptekno.2015.7374104

Kazanci, H.O.: Non-contact head laser tomography. Opt. Quantum Electron. **48**, 330 (2016a). https://doi.org/10.1007/s11082-016-0603-1

Kazanci, H.O.: Head model weight functions generation for laser tomography. Opt. Quantum Electron. **48**, 248 (2016b). https://doi.org/10.1007/s11082-016-0526-x

Kazanci, H.O.: Forward model for cranial laser tomography system. Opt. Quantum Electron. **48**, 39 (2016c). https://doi.org/10.1007/s11082-016-0664-1

Kazanci, H.O.: Image reconstruction for head laser tomography system—Kafa Lazer Tomografi Sistemi İçin Görüntü Oluşturma Algoritması. Ibni Sina J. Med. Sci. İbni Sina Tıp Bilimleri Dergisi **2**(4), 51–55 (2016d)

Kazanci, H.O., Canpolat, M.: Mathematical method for diffuse optical tomography imaging: a research study. El-Cezerî J. Sci. Eng. **1**(3), 40–48 (2014)

Kazanci, H.O., Canpolat, M.: Depth normalization algorithm for continuous wave reflectance diffuse optical tomography system. El-Cezerî J. Sci. Eng. **2**(1), 40–46 (2015a)

Kazanci, H.O., Canpolat, M.: Continuous wave diffuse optical tomography system with high resolution current to voltage analog digital converter. El-Cezerî J. Sci. Eng. **2**(1), 68–77 (2015b)

Kazanci, H.O., Jacques, S.L.: Diffuse light tomography to detect blood vessels using Tikhonov regularization. In: Proceedings of SPIE—Saratov Fall Meetings SFM'15, Optical Technologies in Biophysics and Medicine XVIII; 2015 September 21–25, Saratov State University, Saratov, Russia, (2015)

Kazanci, H.O., Oduncuoglu, M.: Analysis of lung tissue by laser tomography. El Cezeri J. Sci. Eng. **2**(3), 75–81 (2015)

Kazanci, H.O., Oduncuoglu, M.: Design of electronic data acquisiton unit for laser tomography system. El-Cezerî J. Sci. Eng. **3**(4), 1–10 (2016)

Kazanci, H.O., Mercan, T., Canpolat, M.: Design and evaluation of a reflectance diffuse optical tomography system. Opt. Quantum Electron. **47**(2), 257–265 (2015)